

Continually Evolving Skill Knowledge in Vision Language Action Model

Yuxuan Wu^{1,2}, Guangming Wang³, Zhiheng Yang⁴, Maoqing Yao⁵, Brian Sheil³, Hesheng Wang^{1,†}
¹ Shanghai Jiao Tong University, ² Shanghai Innovation Institute, ³ University of Cambridge,
⁴ Beihang University, ⁵ AgiBot

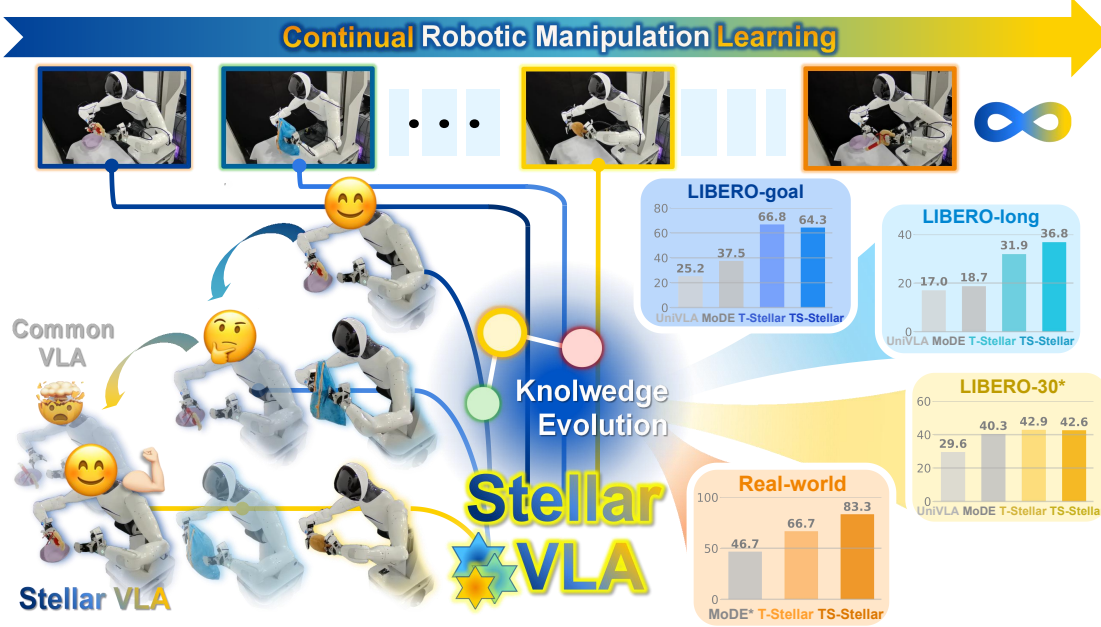


Figure 1. We present **Stellar VLA**, a continual learning VLA framework driven by a self-evolving knowledge space. Its variants T-Stellar and TS-Stellar demonstrate superior final average success rates over UniVLA [6] and MoDE [35].

Abstract

Developing general robot intelligence in open environments requires continual skill learning. Recent Vision-Language-Action (VLA) models leverage massive pretraining data to support diverse manipulation tasks, but they still depend heavily on task-specific fine-tuning, revealing a lack of continual learning capability. Existing continual learning methods are also resource-intensive to scale to VLA models. We propose **Stellar VLA**, a knowledge-driven continual learning framework with two variants: *T-Stellar*, modeling task-centric knowledge space, and *TS-Stellar*, capturing hierarchical task-skill structure. **Stellar VLA** enables self-supervised knowledge evolution through joint learning of task latents and the knowledge space, reducing annotation needs. Knowledge-guided expert routing provide task specialization without extra network parameters, lowering training overhead. Experiments on the

LIBERO benchmark and real-world tasks show over 50% average improvement in final success rates relative to baselines. *TS-Stellar* further excels in complex action inference, and in-depth analyses verify effective knowledge retention and discovery. Our code will be released soon.

1. Introduction

A core requirement for lifelong agents is continual learning that preserves prior knowledge while adapting to new situations. Vision-language-action (VLA) models have advanced robotic policy learning through large-scale pretraining [6, 19]. However, unlike vision or language foundation models that generalize across tasks, they still rely heavily on task-specific fine-tuning [18, 20, 24], reflecting limited understanding of underlying skill relations. The diversity of manipulation skills and environmental complexity make continual learning a key challenge for VLA models toward general robotic intelligence.

Many prior works have explored continual imitation learning (CIL), where agents acquire new skills from

[†] Corresponding author.

demonstrations without forgetting old ones. However, most rely on task-specific adapters or handcrafted features [22, 28, 44, 45], limiting scalability to large VLA with many tasks and parameters. Recent task-centric representation methods [23, 31, 46] address this by improving cross-task generalization via generative modeling, yet their multi-stage training and manual annotation still hinder continual learning. LEGION [30] further extends continual reinforcement learning with an infinite task knowledge space, offering insights for extending CIL to general VLA models.

Mixture-of-Experts (MoE) architectures [38] have also shown strong scalability across multimodal tasks [7, 10, 14, 26, 49]. By dynamically routing among experts, MoE mitigates task interference and scales efficiently, potentially alleviating catastrophic forgetting [45]. These advances raise a key question: Can VLA uncover their latent task-relevant knowledge and leverage it for continual policy evolution through adaptive task specialization?

To explore this question, we propose Stellar VLA, an end-to-end framework for continual imitation learning in vision-language-based manipulation. Stellar VLA enables knowledge evolution through the mutual refinement of task-centric representations and a self-evolving knowledge space, forming a self-supervised cycle of knowledge retention and discovery. Inspired by LEGION [30], we adopt a Dirichlet Process-based variational model to adaptively represent infinite task-relevant knowledge. By integrating task knowledge into expert routing in the action head, the model balances parameter sharing and specialization across tasks. We further introduce two variants: T-Stellar, focused on continual task-centric adaptation, and TS-Stellar, which additionally models hierarchical task-skill relations for reusable skill discovery.

We evaluate our approach in both simulation and real-world settings. On LIBERO benchmark, though trained from scratch, T-Stellar and TS-Stellar achieve strong overall performance, with average final success rates approximately 1.5× higher than those of the baselines [6, 35]. Real-world experiments further confirm these gains, where both variants outperform baselines and TS-Stellar, in particular, shows clear advantages in modeling complex hierarchical actions. Visualizations illustrate their ability to acquire new skills and preserve prior ones. To conclude our contribution:

- We present **Stellar VLA**, a continual imitation learning framework that jointly learns task-centric representations and a self-evolving knowledge space. Two variants are introduced: **T-Stellar** for task-level modeling and **TS-Stellar** for hierarchical task-skill modeling.
- We adopt a knowledge-guided expert routing mechanism, enabling balanced parameter sharing and specialization.
- Experiments on LIBERO and real-world tasks show robust improvements in task adaptation, with both variants capturing evolving task or skill structure.

2. Related Work

Continual Imitation Learning in Robotics. To address catastrophic forgetting in data-driven robotic policy learning, many studies explore Continual Imitation Learning (CIL) [22, 42]. One line of research mitigates forgetting by introducing additional parameters for each new learning phase [22, 25, 28, 29, 34, 36, 45], while another relies on handcrafted task decomposition through clustering or multi-stage learning [22, 44]. However, when scaled to large VLA models covering diverse tasks, the former causes parameter explosion, whereas the latter incurs heavy computation and preprocessing costs due to multimodal data complexity.

Task-centric Representation Learning.

Task-centric representation learning offers the potential for continual skill accumulation in robots. Prior studies [15, 16, 23, 31, 56] have explored action representation learning. VQ-VLA [46] recently extended this idea to large-scale VLA models, enabling unified action tokenization across modalities. However, these methods typically rely on two-stage training comprising action reconstruction and policy learning, resulting in high computational cost.

Recent studies [3, 12, 47, 48, 54] also learn task-centric representations from visual observations and language goals. UniVLA [6] exemplifies this direction by predicting future frames and subgoals. Some work [11, 50] provide unified frameworks for analyzing representation strategies. [50] proves vision-driven features excel in cluttered scenes, and VLA-OS [11] takes an initial step toward continual learning with language and visual grounding. However, most methods still rely on task segmentation or grounding, requiring extensive manual annotation.

LEGION [30] applies a Dirichlet Process Mixture Model [1] for language task representation, forming an infinite knowledge space that enables strong continual reinforcement learning. Despite state priors, it highlights the potential of representation learning for cross-task retention.

In this work, we learn task-centric representations from vision-language data to unify perception and task intent. Motivated by LEGION, a self-evolving knowledge space is proposed to enable automatic knowledge acquisition, reducing dependence on manual annotations.

Policy Models with Mixture of Experts. Recent studies show that the Mixture-of-Experts (MoE) architecture [38] effectively enhances model scalability and computation efficiency in both large language [7, 10, 14] and vision-language models [26, 40, 49]. Recently, VLA models have also incorporated MoE structures to enhance task scalability. MoDE [35] first introduces a diffusion-based MoE policy, where expert routing is determined by noise level rather than task semantics. Many subsequent studies [39, 51–53, 55] leverage MoE for task specialization and improved multitask performance, yet their exploration of continual learning remains limited. SDP [45], though not leverag-

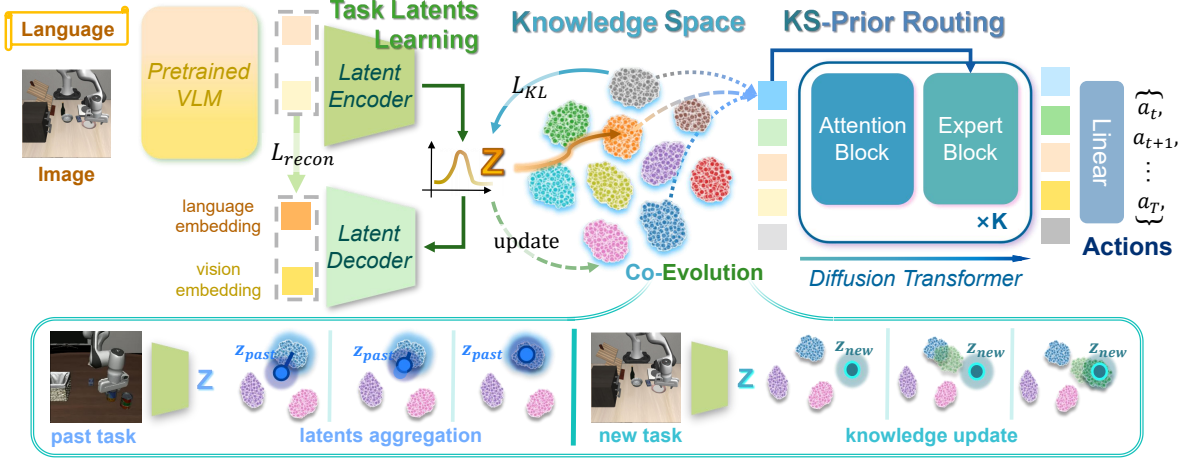


Figure 2. **Overall architecture of Stellar VLA.** CLIP [33] and FiLM [32]-conditioned ResNet encode language and visual inputs respectively. The task-centric representation z and knowledge space are jointly learned through knowledge update and latents aggregation, as detailed in Sec. 3.3. The learned knowledge prior finally guides the MoE action head for motion prediction, as detailed in Sec. 3.4.

ing language information, demonstrates the potential of MoE structures for continual learning by introducing task-specific routers to reduce parameter interference. However, its experts mainly operate in perception modules and require additional expert layers for incremental adaptation. In this work, we propose a fixed-size task-specific MoE action head guided by priors from knowledge space, leveraging the strengths of MoE to enhance continual learning.

3. Method

In this section, we present the architecture of Stellar VLA (Fig. 2), which enables CIL for vision-language manipulation. Our goal is to continually evolve task-relevant knowledge, enabling Stellar VLA to acquire new skills while mitigating forgetting of prior tasks. We first define the CIL setting, then describe the design and evolution of the knowledge space, and finally explain the process of guiding the expert policy via knowledge priors.

3.1. Problem Formulation

In the CIL setting [22], an agent learns sequentially from a stream of tasks $\{\mathcal{T}_j\}_{j=1}^{\infty}$, where each task j provides N expert demonstrations $\{\tau_j^i\}_{i=1}^N$, consisting of language instructions l , observations o , and actions a . Unlike multi-task learning assuming full access to all demonstrations, CIL requires acquiring new task knowledge under limited access to past data while retaining previously learned skills, reflecting the realistic demands of lifelong robot learning.

To alleviate forgetting caused by limited access to past tasks, following LOTUS [44], we adopt Experience Replay (ER) with a small buffer \mathcal{B} . After completing task j , $q\%$ of its demonstrations are stored in \mathcal{B} and jointly trained with

current data when learning task $j+1$. However, relying on only a small portion of past data often leads to prediction drift on previous tasks \mathcal{T}_k ($k < j+1$). To address this, we design a VLA architecture that continually discovers and preserves task knowledge, enabling dynamic expert composition for better parameter sharing and reduced interference.

3.2. Dirichlet-Process-based Knowledge Space

To capture both shared and distinct patterns across tasks, merely learning task-centric representations [23, 31, 46] is insufficient. Latent representations describe task-relevant variations after filtering sensory noise, but remain low-level abstractions without explicit task affiliation, making it difficult to separate new from past tasks and often leading to catastrophic forgetting during continual learning. To obtain discrete and interpretable task- or skill-level knowledge, these representations are further organized into a high-level, dynamically evolving knowledge space.

In CIL, task-relevant knowledge would incrementally grow as new task data arrives. Finite parametric models, such as Gaussian Mixture Models [4], cannot adaptively fit the expanding knowledge space. Following LEGION [30], we adopt a Dirichlet Process (DP)-based nonparametric model that allows infinite mixture clustering.

Dirichlet-Process Model. In DP, the sampling process $G \sim DP(\alpha, G_0)$ can be written as:

$$G = \sum_{k=1}^{\infty} \pi_k \delta_{\theta_k^*}, \quad \theta_k^* \sim G_0, \quad (1)$$

Here, G is a probability measure and G_0 the base distribution. θ_k^* are distribution parameters, while π_k are infinite-dimensional weights [37]. Considering G_0 as the aggregated knowledge of infinite tasks, then G could represent a

random measure over the current task set. The discreteness of G causes samples θ from G to repeat, naturally forming clusters. Moreover, its nonparametric property allows new clusters to emerge as needed, making the knowledge space inherently open and self-evolving.

Building on DP-based clustering, we design two knowledge spaces: 1) a task-centric space using Dirichlet Process Mixture Model (DPMM) to form task clusters from the latent representations, and 2) a hierarchical task-skill space using a Hierarchical Dirichlet Process (HDP) to capture task-skill relations.

Task-Centric Knowledge Modeling from DPMM. Task distributions in latent space are dynamically clustered using Dirichlet Process Mixture Model (DPMM), a Bayesian nonparametric model supporting potentially infinite clusters.

In DPMM, based on DP sampling in Eq. (1), the full generative process for z_j in task j under the task-set probability measure G can be expressed as $z_j \sim F_{task}(\theta_j)$, $\theta_j \sim G$, where θ_j denotes the distribution parameters for task j sampled from G , and $F_{task}(\theta_j)$ represents its corresponding observation model. Thus, sampling from DPMM corresponds to drawing a latent observation from a task distribution. Assuming F_{task} is Gaussian, the DPMM models a knowledge space comprising an unbounded set of task-centric Gaussian distributions based on latent task representations.

Hierarchical Task-Skill Knowledge Modeling from HDP. The DPMM-based knowledge space assumes independent task distribution from z_j . However, robotic tasks often share subskills, and DPMM alone may fail to capture these relations in complex or long-horizon settings. To model such hierarchy, we extend it with a Hierarchical Dirichlet Process (HDP) [41].

Specifically, each task j is modeled as a probability measure over its subset of skills $\{\text{skill}_i\}$. Thus, by applying a second-level DP sampling on the task-set measure G , we could obtain skill distribution parameters θ_{ji} and corresponding latent skill samples z_{ji} in task j as:

$$z_{ji} \sim F_{skill}(\theta_{ji}), \theta_{ji} \sim G_j, G_j \sim DP(\gamma, G) \quad (2)$$

Assuming F_{skill} as a Gaussian distribution, each skill i could be parameterized by $\theta_i^{skill} = (\mu_i^{skill}, \sigma_i^{skill})$. The distribution parameters of each task, $\theta_j^{task} = (\mu_j^{task}, \sigma_j^{task})$, can be derived from its associated skill set $\{\text{skill}_i\}$:

$$\begin{aligned} \mu_j^{task} &= \sum_{\text{skill } i \in \text{task } j} \pi_{ji} \mu_i^{skill}, \\ \sigma_j^{task^2} &= \sum_{\text{skill } i \in \text{task } j} \pi_{ji} [\sigma_i^{skill^2} + (\mu_i^{skill} - \mu_j^{task})^2]. \end{aligned} \quad (3)$$

π_{ji} is the local mixture weight of skill i in task j . According to Eq. (1), task-level probability measure G_j would share atoms θ_k with G , but has different mixture weights. This formulation naturally models shared skills across tasks, forming a hierarchical task-skill knowledge space.

3.3. Knowledge Space Learning via Self-Evolution

This section presents the co-evolution of the knowledge space with Stellar VLA during CIL, resulting in two variants: T-Stellar and TS-Stellar, based on task-centric and task-skill hierarchical knowledge spaces respectively.

Following Sec. 3.2, we consider the dependency chain from sensor observations through latent representations to the knowledge space. To finally get stable knowledge features, a hierarchical variational inference is performed: task-centric latent representations are inferred via VAE [21] from vision-language data for new task learning, and task knowledge is inferred from them through DP-base models to manage old and new task information.

Task-Centric Representation Learning. To obtain semantically rich task-centric representations z_j for task j , we employ a VAE that reconstructs vision-language inputs. Unlike standard VAE that learn latents from a predefined Gaussian prior, z_j is constrained to aggregate within the task-relevant knowledge space as shown in Fig. 2, thus reducing forgetting of past experiences. Specifically, the model is trained by minimizing the reconstruction loss L_{recon} and KL divergence L_{kl} , with task-specific adaptations for knowledge-space alignment.

In T-Stellar, the language goal l and observation o serves as the reconstruction target. L_{kl} is computed from the probability p_{jk} of z_j^{task} belonging to Gaussian cluster k .

$$L_{KL_j} = \sum_{k=1}^{K_c} p_{jk} L_{KL_{jk}} \quad (4)$$

Here, K_c is the number of clusters in the current DPMM, and $L_{KL_{jk}}$ is the KL divergence between z_j and cluster k , measuring the similarity between the task-centric representation and DPMM components.

For TS-Stellar which hierarchically models tasks and skills, we use a hierarchical VAE to approximate their latent vectors. The task representation z_j^{task} from the encoder is passed through linear layers along with visual embeddings to generate skill representation z_j^{skill} . The reconstruction loss L_{recon}^{TS} is then given by:

$$L_{recon}^{TS} = L_{recon}(f_{dec}^{task}(z_j^{task}), l_j) + L_{recon}(f_{dec}^{skill}(z_j^{skill}), o_j) \quad (5)$$

which measures encoding of language l via z_j^{task} and observation o via z_j^{skill} . Visual observations implicitly capture task-related skills. For L_{kl} , HDP defines task- and skill-level losses: task parameters are obtained from known skill clusters (Eq. (3)), and L_{kl}^{HDP} sums the KL divergences between $(z_j^{task}, \{\theta^{task}\})$, and $(z_j^{skill}, \{\theta^{skill}\})$:

$$\mathcal{L}_{KL_j}^{TS} = \mathcal{L}_{KL_j}(z_j^{task}, \theta^{task}) + \mathcal{L}_{KL_j}(z_j^{skill}, \theta^{skill}) \quad (6)$$

Knowledge Space Distribution Learning. As task-centric representations are continuously learned from vision-language observations under the constraints of DP

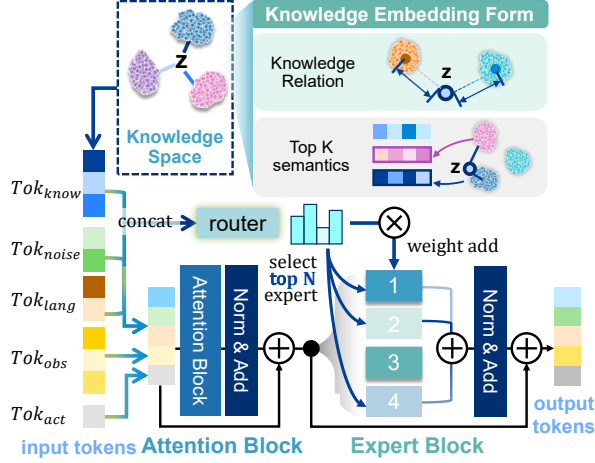


Figure 3. **Knowledge-prior-routed MoE action head.** Two knowledge embeddings, relation and top-K semantic, are computed for expert routing, alongside language, noise, observation and noise action tokens fed into the denoising transformer.

models, the DP-based knowledge space is simultaneously updated based on these representations, ensuring timely discovery of new knowledge, as illustrated in Fig. 2. Considering z_j as observations of the knowledge space, we perform variational inference to approximate the posterior $p(\theta_j, G \mid z_j)$ of the DP mixture. Posterior estimation is conducted via the memory-based Variational Bayes (mem-oVB) [13] algorithm, which supports incremental learning by sharing global statistics across tasks.

During VLA training, our task-centric representation learning and knowledge space updating are jointly performed in a fully self-supervised manner. The perception encoder continuously provides latent features to update the knowledge distribution, while the knowledge space, via KL loss L_{kl} , constrains z_j to infer under task or skill hypotheses. This design establishes a self-evolving cycle that autonomously retains and discovers knowledge over time.

3.4. Action-Knowledge-guided Expert Routing

After learning the knowledge space and task-centric latents, we introduce a knowledge-routed MoE module to allocate task-specific action prediction parameters, minimizing interference between unrelated tasks while enhancing sharing among related ones. A diffusion-based MoE action head is adopted referring to MoDE [35], replacing linear layers in the denoising transformer with MoE modules:

$$\text{MoE}(tok, \mathbf{f}_{ro}) = \sum_{i=1}^{N_e} \text{Router}_i(\mathbf{f}_{ro}) \cdot \text{Expert}_i(tok) \quad (7)$$

Here, tok is the input token feature tensor and \mathbf{f}_{ro} the routing features, defined in MoDE as the noise embed-

ding $\mathbf{f}_{router} = tok_{noise} = \phi(\sigma_t)$. Unlike MoDE’s noise-level routing, we guide expert allocation via the knowledge space, enabling continual task learning with task-specific parameter sharing and differentiation. Since DPMM and HDP produce variable numbers of clusters, directly feeding their task distributions into a fixed-dimension network is impractical. Thus, we design two knowledge embedding formats, as shown in Fig. 3.

Knowledge Relation Embedding encodes the distance between latent z and cluster centers μ_k . Given the membership probability p_k of z for cluster k as described in Sec. 3.3, relation embedding is computed as:

$$\mathbf{f}_R = \sum_{k=1}^{K_c} p_k |z - \mu_k| \quad (8)$$

Top-K Semantic Embedding represents the discrete skill semantic affiliation of z by aggregating learnable embeddings of the top-K assigned clusters:

$$\mathbf{f}_S = \sum_{k \in \mathcal{I}_T} p_k \cdot \text{Embed}(k), \mathcal{I}_T = \text{TopKIndice}(p_1, \dots, p_K, z) \quad (9)$$

Finally, the embedded knowledge of current task and skill could be represented as:

$$\mathbf{f}_{\text{know}} = [z \parallel \mathbf{f}_R \parallel \mathbf{f}_S] \quad (10)$$

The knowledge embedding \mathbf{f}_{know} is introduced as an additional guidance token tok_{know} , which, together with noise token tok_{noise} and language token tok_{lang} , are concatenated to feed the router for task-aware expert allocation.

By incorporating knowledge space guidance into expert routing, the model could achieve effective CIL through balanced parameter sharing and isolation, enabling related tasks to benefit from shared experience while preventing catastrophic forgetting across dissimilar ones.

4. Experiments

Our experiments address four questions: (I) Can T-Stellar and TS-Stellar surpass state-of-the-art VLA models in end-to-end continual learning? (II) Does TS-Stellar’s hierarchical task-skill knowledge space outperform T-Stellar’s task-only modeling? (III) Do DP-based knowledge space and knowledge-guided expert routing enhance continual learning? (IV) How does the DP-based knowledge space gradually discover and preserve skills?

4.1. Simulation Experiments

We evaluate our models on the LIBERO benchmark [27], including LIBERO-goal, LIBERO-long, and LIBERO-30*, a 30-task subset of LIBERO-90 constructed by ourselves, for comprehensive evaluation under diverse goals, long-horizon reasoning, and a large number of tasks. Demo data

Table 1. **Overall performance on the LIBERO benchmark.** Baselines are grouped into pretrained and scratch categories. Results are reported in percentages. The best scratch model is shown in **bold**, and the best overall in underline.

tasks	metrics	UniVLA [6] (fine-tuned)	MoDE [35] (fine-tuned)	MoDE [35] (scratch)	T-Stellar (scratch, ours)	TS-Stellar (scratch, ours)
LIBERO-goal	FWT (\uparrow)	87.4	69.7	68.5	81.9	78.5
	NBT (\downarrow)	59.6	27.9	33.6	19.3	21.9
	AUC (\uparrow)	39.9	43.3	38.5	63.2	58.3
	Final SR (\uparrow)	25.2	37.5	36.0	66.8	64.3
LIBERO-long	FWT (\uparrow)	70.6	68.3	66.6	78.6	74.7
	NBT (\downarrow)	32.38	45.7	45.4	44.3	37.9
	AUC (\uparrow)	<u>44.97</u>	30.6	28.4	41.2	41.7
	Final SR (\uparrow)	17.0	18.7	18.6	31.9	36.8
LIBERO-30 *	FWT (\uparrow)	<u>87.9</u>	52.9	48.2	79.6	73.3
	NBT (\downarrow)	57.7	<u>11.9</u>	15.4	31.0	27.8
	AUC (\uparrow)	36.5	43.0	33.6	49.7	48.3
	Final SR (\uparrow)	29.6	40.3	28.5	42.9	42.6

Table 2. **Performance on real-world experiments.** MoDE* is our modified MoDE [35] for dual arm tasks, and all models are trained from scratch. The best performance is highlighted in **bold**. All models are trained from scratch.

tasks	metrics	MoDE* [35]	T-Stellar	TS-Stellar
Dual arm real world task	FWT (\uparrow)	96.7	96.7	96.7
	NBT (\downarrow)	45.0	35.0	21.7
	AUC (\uparrow)	69.4	76.1	82.2
	Final SR (\uparrow)	46.7	66.7	83.3

consist of static and wrist camera images, and actions include end-effector poses and gripper states.

For continual learning, models are trained sequentially following the task order in LIBERO, using Experience Replay with only 1% of past data stored, which suffices for LIBERO tasks while reducing memory overhead. Both T-Stellar and TS-Stellar are trained from scratch.

Baselines. Since no VLA has been evaluated under CIL, we select strong multitask performers on LIBERO and re-train them under this setting for fair comparison. The baselines include: 1) Pretrained UniVLA [6], which learns task-centric representations via large-scale latent action pretraining and achieves state-of-the-art multitask results; 2) MoDE [35], a diffusion-based Mixture-of-Experts VLA similar to our action head, serving as a key comparison. Both pretrained and scratch variants are evaluated, consistent with its original setups.

Metrics. We evaluate continual learning using four metrics: FWT (forward transfer), NBT (negative backward transfer), AUC (area under the success rate curve), [8, 22, 27, 44] and Final SR (final average success rate), all computed from the success rate matrix R where $R_{i,j}$ is the success on task j after learning i tasks. FWT measures forward learning, NBT measures forgetting, AUC reflects overall

performance stability, and Final SR is overall success after training all tasks. Formally, $FWT = \frac{1}{M} \sum_{m=1}^M R_{m,m}$, $NBT = \frac{1}{M} \sum_{m=1}^M \frac{1}{M-m} \sum_{q=m+1}^M (R_{m,m} - R_{q,m})$, $AUC = \frac{1}{M} \sum_{m=1}^M \frac{1}{M-m+1} \left(R_{m,m} + \sum_{q=m+1}^M R_{q,m} \right)$, $Final\ SR = \frac{1}{M} \sum_{j=1}^M R_{M,j}$. Each policy is evaluated on all previous tasks 100 times to form the SR matrix.

Results. Tab. 1 shows that T-Stellar and TS-Stellar achieve the highest final success rates across all scenarios, with over 50% average improvement relative to both pretrained and from-scratch baselines [6, 35]. They also outperform most baselines in AUC and NBT, demonstrating strong and stable continual learning performance.

Among baselines, UniVLA is the most competitive, benefiting from its large model capacity and unified action space, which yield strong FWT and long-horizon performance. However, without explicit task-specific knowledge and task-guided action allocation, it suffers from poor retention in single-scene and many-task scenarios, often showing highest NBT and lowest Final SR, highlighting the instability of current VLA models under continual learning.

Compared with both fine-tuned and from-scratch MoDE, our methods achieve the best FWT and AUC across all settings. MoDE variants achieve better NBT on LIBERO-30, mainly because their FWT is only about half of ours, resulting in lower retention pressure. This reflects the inherent trade-off between strong forward transfer and maintaining low backward transfer in continual learning.

Therefore, in response to Question (I), although trained from scratch, our methods consistently outperform both pretrained and from-scratch VLA models in overall continual learning. Notably, TS-Stellar surpasses T-Stellar on long-horizon tasks but slightly lags on simpler tasks, likely because the advantages of hierarchical task-skill modeling are less pronounced in such settings.

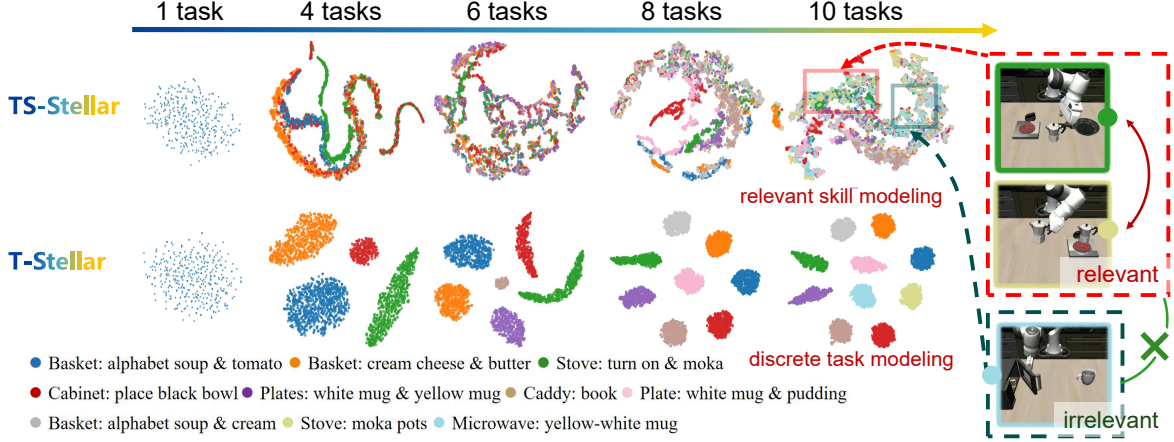


Figure 4. **T-SNE visualization of Stellar VLA** Latent representations after 1, 4, 6, 8, and 10 tasks on LIBERO-long are shown. Task names are abbreviated for clarity. T-Stellar models discrete task distributions, and TS-Stellar learn relevant skill across tasks.

Table 3. **Knowledge space ablation experiments on LIBERO and real-world tasks.** The best performance is shown in **bold**.

tasks	metrics	w/o VAE	w/o KS	T-Stellar	TS-Stellar
LIBERO-goal	FWT (\uparrow)	70.8	76.6	81.9	78.5
	NBT (\downarrow)	30.1	21.9	19.3	21.9
	AUC (\uparrow)	43.5	56.4	63.2	58.3
	Final SR (\uparrow)	36.2	43.8	66.8	64.3
LIBERO-long	FWT (\uparrow)	60.9	73.5	78.6	74.7
	NBT (\downarrow)	38.9	47.0	44.3	37.9
	AUC (\uparrow)	27.2	34.5	41.2	41.7
	Final SR (\uparrow)	17.1	22.0	31.9	36.8
LIBERO-30 *	FWT (\uparrow)	45.0	45.1	79.6	73.3
	NBT (\downarrow)	12.0	4.9	31.0	27.8
	AUC (\uparrow)	32.7	38.9	49.7	48.3
	Final SR (\uparrow)	26.3	35.8	42.9	42.6
Dual arm real world task	FWT (\uparrow)	90.0	96.7	96.7	96.7
	NBT (\downarrow)	55.0	58.3	31.0	27.8
	AUC (\uparrow)	58.9	63.3	76.1	82.2
	Final SR (\uparrow)	36.7	40.0	66.7	83.3

4.2. Real-Word Experiment

To further evaluate real-world effectiveness, we conduct dual-arm manipulation experiments on a humanoid robot platform. Three tasks are designed as a continual learning sequence: 1) “Transfer Magic Stick”, 2) “Pick up Bag”, and 3) “Handover Toy”. Models are trained sequentially with a 5% replay rate for stability. Observations are collected from a head camera and dual wrist cameras, while outputs consist of joint poses and gripper states. Evaluation follows Sec. 4.1, with each task tested ten times.

Baselines. As mentioned, MoDE [35] serves as a key reference for our method. However, since MoDE was originally designed for single-arm Cartesian action prediction, we modified its architecture without altering core components to ensure fair comparison on dual-arm joint-space tasks. The modified trained from scratch version is denoted

Table 4. **Prior-guided expert routing ablation experiments on LIBERO-long.** The best performance is highlighted in **bold**.

tasks	metrics	T-Stellar w/o K-route	T-Stellar	TS-Stellar w/o K-route	TS-Stellar
LIBERO-long	FWT (\uparrow)	74.4	78.6	76.1	74.7
	NBT (\downarrow)	44.1	44.3	42.7	37.9
	AUC (\uparrow)	38.0	41.2	39.4	41.7
	Final SR (\uparrow)	20.9	31.9	30.8	36.8

as MoDE*, and its pretrained model is thus not used.

Results. FWT, NBT, AUC and Final SR are reported in Tab. 2. The results show that T-Stellar and TS-Stellar substantially outperform MoDE* in NBT, AUC, and Final SR while achieve strong FWT, demonstrating superior continual learning on dual-arm real-world tasks. TS-Stellar further surpasses T-Stellar across all these metrics, suggesting that task–skill modeling is particularly effective for long-horizon skill sequences and complex action mappings, thus addressing Question (II).

4.3. Ablation Studies

In this section, we conduct two sets of ablation studies to investigate the effectiveness of the proposed knowledge space and expert routing mechanisms.

Knowledge Space Ablation. We perform ablations by replacing the DP-based knowledge space with a standard Gaussian ($\mu = 0, \sigma = 1$) (w/o KS) and by removing latent task-centric representation learning (w/o VAE). Experiments are conducted across all simulation and real-world tasks, as shown in Tab. 3. Results demonstrate that our DP-based knowledge spaces significantly improve all four metrics—except for NBT on LIBERO-30, which is affected by weaker forward learning of the ablations. Overall, the

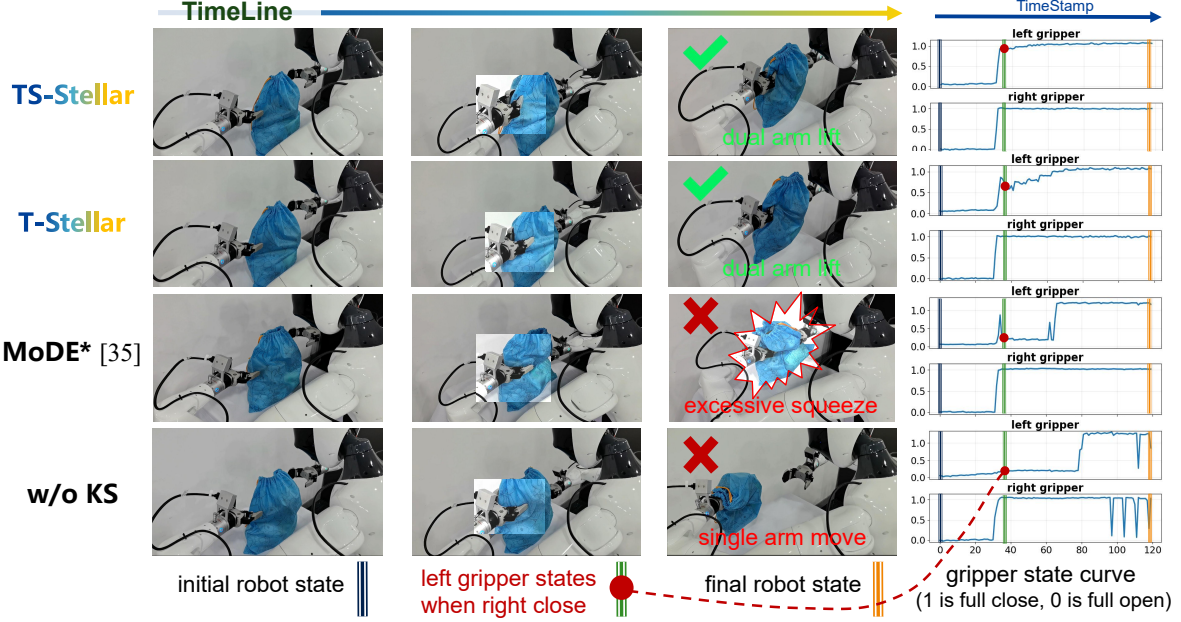


Figure 5. **Behavior visualization on “Pick up Bag” after training on “Handover Toy”.** TS-Stellar achieves the most synchronized dual-arm motion; T-Stellar hesitates slightly; MoDE* and w/o KS show strong desynchronization and ultimately fail.

results validates the effectiveness of our DPMM-based task-centric and HDP-based task-skill knowledge spaces.

Knowledge Guidance for Expert Routing Effectiveness. We evaluate T-Stellar and TS-Stellar on LIBERO-long without the knowledge-guidance token tok_{know} , as shown in Tab. 4. Both models achieve higher AUC and Final SR with knowledge guidance.

Through ablation studies, we could answer Question (III): The DP-based knowledge space enhances continual learning by capturing task and skill distributions for better task separation and knowledge sharing, while knowledge-routed MoE further improves stability and performance through dynamic expert allocation.

4.4. Visualization for Continual Learning process

To demonstrate how the proposed method support continual skill evolution, we visualize the learning process.

Knowledge Evolution During Continual Learning. We analyze knowledge space evolution on LIBERO-long. Fig. 4 shows t-SNE plots of latent representations after training on selected tasks. T-Stellar learns distinct clusters for different tasks, and TS-Stellar connects tasks through shared subskills. For example, deep green and light green tasks overlaps since they share the same “put moka on stove” subgoal.

Execution Behavior Analysis. To understand performance drops during continual learning, we visualize real-world robot actions. Fig. 5 shows the “Pick up Bag” task after “Handover Toy” training for T-Stellar, TS-Stellar,

MoDE*, and w/o KS ablation. For the “Pick up Bag” task, both grippers close synchronously, but asynchrony could emerge after training on “Handover Toy”. TS-Stellar maintains stable, synchronized gripper and arm motion. T-Stellar shows mild hesitation yet still lifts the bag. In contrast, MoDE* and w/o KS exhibit clear gripper desynchronization; MoDE* fails from over-squeezing the bag, while w/o KS fails by rigidly following the action pattern of task “Handover Toy”.

Overall, visualization and behavior analysis answer Question (IV): T-Stellar learns distinct clusters for new tasks, whereas TS-Stellar captures inter-task skill relations, forming an overlapping task-skill knowledge space. Retaining skill priors enables stable old-task execution and mitigates behavioral drift during continual learning.

5. Conclusion

We introduce Stellar VLA, a knowledge space driven policy for continual imitation learning, with two variants: T-Stellar, which constructs task-centric knowledge spaces, and TS-Stellar, which models hierarchical task-skill relations. By leveraging the evolving knowledge space to guide expert selection, our models reduce interference between tasks while enabling continual skill acquisition. Experiments on LIBERO and real-world tasks demonstrate significant performance gains, and visualizations show the effective evolution of task and skill knowledge. Future work could explore larger skill spaces to scale up continual learning for larger VLA models.

References

- [1] Charles E Antoniak. Mixtures of dirichlet processes with applications to bayesian nonparametric problems. *The annals of statistics*, pages 1152–1174, 1974. [2](#)
- [2] Jun Bai, Minghao Tong, Yang Liu, Zixia Jia, and Zilong Zheng. Understanding and leveraging the expert specialization of context faithfulness in mixture-of-experts llms. In *Proceedings of the 2025 Conference on Empirical Methods in Natural Language Processing*, pages 21938–21953, 2025. [5](#)
- [3] Suneel Belkhale, Tianli Ding, Ted Xiao, Pierre Sermanet, Quon Vuong, Jonathan Tompson, Yevgen Chebotar, Debidda Dwibedi, and Dorsa Sadigh. Rt-h: Action hierarchies using language. *arXiv preprint arXiv:2403.01823*, 2024. [2](#)
- [4] Zhenshan Bing, David Lerch, Kai Huang, and Alois Knoll. Meta-reinforcement learning in non-stationary and dynamic environments. *IEEE Transactions on Pattern Analysis and Machine Intelligence*, 45(3):3476–3491, 2022. [3](#)
- [5] David M Blei, Alp Kucukelbir, and Jon D McAuliffe. Variational inference: A review for statisticians. *Journal of the American statistical Association*, 112(518):859–877, 2017. [1](#)
- [6] Qingwen Bu, Yanting Yang, Jisong Cai, Shenyuan Gao, Guanghui Ren, Maoqing Yao, Ping Luo, and Hongyang Li. Univla: Learning to act anywhere with task-centric latent actions. *arXiv preprint arXiv:2505.06111*, 2025. [1](#), [2](#), [6](#), [3](#), [4](#)
- [7] Damai Dai, Chengqi Deng, Chenggang Zhao, RX Xu, Huazuo Gao, Deli Chen, Jishi Li, Wangding Zeng, Xingkai Yu, Yu Wu, et al. Deepseekmoe: Towards ultimate expert specialization in mixture-of-experts language models. *arXiv preprint arXiv:2401.06066*, 2024. [2](#)
- [8] Natalia Diaz-Rodríguez, Vincenzo Lomonaco, David Filliat, and Davide Maltoni. Don’t forget, there is more than forgetting: new metrics for continual learning. *arXiv preprint arXiv:1810.13166*, 2018. [6](#)
- [9] William Fedus, Barret Zoph, and Noam Shazeer. Switch transformers: Scaling to trillion parameter models with simple and efficient sparsity. *Journal of Machine Learning Research*, 23(120):1–39, 2022. [3](#)
- [10] William Fedus, Barret Zoph, and Noam Shazeer. Switch transformers: Scaling to trillion parameter models with simple and efficient sparsity. *Journal of Machine Learning Research*, 23(120):1–39, 2022. [2](#)
- [11] Chongkai Gao, Zixuan Liu, Zhenghao Chi, Junshan Huang, Xin Fei, Yiwen Hou, Yuxuan Zhang, Yudi Lin, Zhirui Fang, Zeyu Jiang, et al. Vla-os: Structuring and dissecting planning representations and paradigms in vision-language-action models. *arXiv preprint arXiv:2506.17561*, 2025. [2](#)
- [12] Shengran Hu and Jeff Clune. Thought cloning: Learning to think while acting by imitating human thinking. *Advances in Neural Information Processing Systems*, 36:44451–44469, 2023. [2](#)
- [13] Michael C Hughes and Erik Sudderth. Memoized online variational inference for dirichlet process mixture models. *Advances in neural information processing systems*, 26, 2013. [5](#), [1](#), [2](#)
- [14] Albert Q Jiang, Alexandre Sablayrolles, Antoine Roux, Arthur Mensch, Blanche Savary, Chris Bamford, Devendra Singh Chaplot, Diego de las Casas, Emma Bou Hanna, Florian Bressand, et al. Mixtral of experts. *arXiv preprint arXiv:2401.04088*, 2024. [2](#)
- [15] Zhengyao Jiang, Tianjun Zhang, Michael Janner, Yueying Li, Tim Rocktäschel, Edward Grefenstette, and Yuandong Tian. Efficient planning in a compact latent action space. *arXiv preprint arXiv:2208.10291*, 2022. [2](#)
- [16] Zhengyao Jiang, Yingchen Xu, Nolan Wagener, Yicheng Luo, Michael Janner, Edward Grefenstette, Tim Rocktäschel, and Yuandong Tian. H-gap: Humanoid control with a generalist planner. *arXiv preprint arXiv:2312.02682*, 2023. [2](#)
- [17] Tero Karras, Miika Aittala, Timo Aila, and Samuli Laine. Elucidating the design space of diffusion-based generative models. *Advances in neural information processing systems*, 35:26565–26577, 2022. [3](#)
- [18] Kento Kawaharazuka, Jihoon Oh, Jun Yamada, Ingmar Posner, and Yuke Zhu. Vision-language-action models for robotics: A review towards real-world applications. *IEEE Access*, 2025. [1](#)
- [19] Moo Jin Kim, Karl Pertsch, Siddharth Karamcheti, Ted Xiao, Ashwin Balakrishna, Suraj Nair, Rafael Rafailov, Ethan Foster, Grace Lam, Pannag Sanketi, et al. Openvla: An open-source vision-language-action model. *arXiv preprint arXiv:2406.09246*, 2024. [1](#)
- [20] Moo Jin Kim, Chelsea Finn, and Percy Liang. Fine-tuning vision-language-action models: Optimizing speed and success. *arXiv preprint arXiv:2502.19645*, 2025. [1](#)
- [21] Diederik P Kingma and Max Welling. Auto-encoding variational bayes. *arXiv preprint arXiv:1312.6114*, 2013. [4](#)
- [22] Daehee Lee, Minjong Yoo, Woo Kyung Kim, Wonje Choi, and Honguk Woo. Incremental learning of retrievable skills for efficient continual task adaptation. *Advances in Neural Information Processing Systems*, 37:17286–17312, 2024. [2](#), [3](#), [6](#)
- [23] Seungjae Lee, Yibin Wang, Haritheja Etukuru, H Jin Kim, Nur Muhammad Mahi Shafiullah, and Lerrel Pinto. Behavior generation with latent actions. *arXiv preprint arXiv:2403.03181*, 2024. [2](#), [3](#)
- [24] Chen Li, Zhantao Yang, Han Zhang, Fangyi Chen, Chenchen Zhu, Anudeepsekhar Bolimera, and Marios Savvides. Metavla: Unified meta co-training for efficient embodied adaption. *arXiv preprint arXiv:2510.05580*, 2025. [1](#)
- [25] Xilai Li, Yingbo Zhou, Tianfu Wu, Richard Socher, and Caiming Xiong. Learn to grow: A continual structure learning framework for overcoming catastrophic forgetting. In *International conference on machine learning*, pages 3925–3934. PMLR, 2019. [2](#)
- [26] Bin Lin, Zhenyu Tang, Yang Ye, Jiaxi Cui, Bin Zhu, Peng Jin, Jinfa Huang, Junwu Zhang, Yatian Pang, Munan Ning, et al. Moe-llava: Mixture of experts for large vision-language models. *arXiv preprint arXiv:2401.15947*, 2024. [2](#)
- [27] Bo Liu, Yifeng Zhu, Chongkai Gao, Yihao Feng, Qiang Liu, Yuke Zhu, and Peter Stone. Libero: Benchmarking knowledge transfer for lifelong robot learning. *Advances in Neural*

- Information Processing Systems*, 36:44776–44791, 2023. 5, 6
- [28] Zuxin Liu, Jesse Zhang, Kavosh Asadi, Yao Liu, Ding Zhao, Shoham Sabach, and Rasool Fakoor. Tail: Task-specific adapters for imitation learning with large pretrained models. *arXiv preprint arXiv:2310.05905*, 2023. 2
 - [29] Arun Mallya and Svetlana Lazebnik. Packnet: Adding multiple tasks to a single network by iterative pruning. In *Proceedings of the IEEE conference on Computer Vision and Pattern Recognition*, pages 7765–7773, 2018. 2
 - [30] Yuan Meng, Zhenshan Bing, Xiangtong Yao, Kejia Chen, Kai Huang, Yang Gao, Fuchun Sun, and Alois Knoll. Preserving and combining knowledge in robotic lifelong reinforcement learning. *Nature Machine Intelligence*, pages 1–14, 2025. 2, 3
 - [31] Atharva Mete, Haotian Xue, Albert Wilcox, Yongxin Chen, and Animesh Garg. Quest: Self-supervised skill abstractions for learning continuous control. *Advances in Neural Information Processing Systems*, 37:4062–4089, 2024. 2, 3
 - [32] Ethan Perez, Florian Strub, Harm De Vries, Vincent Dumoulin, and Aaron Courville. Film: Visual reasoning with a general conditioning layer. In *Proceedings of the AAAI conference on artificial intelligence*, 2018. 3, 2
 - [33] Alec Radford, Jong Wook Kim, Chris Hallacy, Aditya Ramesh, Gabriel Goh, Sandhini Agarwal, Girish Sastry, Amanda Askell, Pamela Mishkin, Jack Clark, et al. Learning transferable visual models from natural language supervision. In *International conference on machine learning*, pages 8748–8763. PmLR, 2021. 3, 2
 - [34] Dushyant Rao, Francesco Visin, Andrei Rusu, Razvan Pascanu, Yee Whye Teh, and Raia Hadsell. Continual unsupervised representation learning. *Advances in neural information processing systems*, 32, 2019. 2
 - [35] Moritz Reuss, Jyothish Pari, Pulkit Agrawal, and Rudolf Lioutikov. Efficient diffusion transformer policies with mixture of expert denoisers for multitask learning. *arXiv preprint arXiv:2412.12953*, 2024. 1, 2, 5, 6, 7, 3, 4
 - [36] Andrei A Rusu, Neil C Rabinowitz, Guillaume Desjardins, Hubert Soyer, James Kirkpatrick, Koray Kavukcuoglu, Razvan Pascanu, and Raia Hadsell. Progressive neural networks. *arXiv preprint arXiv:1606.04671*, 2016. 2
 - [37] Jayaram Sethuraman. A constructive definition of dirichlet priors. *Statistica sinica*, pages 639–650, 1994. 3, 1
 - [38] Noam Shazeer, Azalia Mirhoseini, Krzysztof Maziarsz, Andy Davis, Quoc Le, Geoffrey Hinton, and Jeff Dean. Outrageously large neural networks: The sparsely-gated mixture-of-experts layer. *arXiv preprint arXiv:1701.06538*, 2017. 2
 - [39] Weijie Shen, Yitian Liu, Yuhao Wu, Zhixuan Liang, Sijia Gu, Dehui Wang, Tian Nian, Lei Xu, Yusen Qin, Jiangmiao Pang, et al. Expertise need not monopolize: Action-specialized mixture of experts for vision-language-action learning. *arXiv preprint arXiv:2510.14300*, 2025. 2
 - [40] Kimi Team, Angang Du, Bohong Yin, Bowei Xing, Bowen Qu, Bowen Wang, Cheng Chen, Chenlin Zhang, Chen-zhuang Du, Chu Wei, et al. Kimi-vl technical report. *arXiv preprint arXiv:2504.07491*, 2025. 2
 - [41] Yee Whye Teh, Michael I Jordan, Matthew J Beal, and David M Blei. Hierarchical dirichlet processes. *Journal of the american statistical association*, 101(476):1566–1581, 2006. 4
 - [42] Sebastian Thrun and Tom M Mitchell. Lifelong robot learning. *Robotics and autonomous systems*, 15(1-2):25–46, 1995. 2
 - [43] Pascal Vincent. A connection between score matching and denoising autoencoders. *Neural computation*, 23(7):1661–1674, 2011. 3
 - [44] Weikang Wan, Yifeng Zhu, Rutav Shah, and Yuke Zhu. Lotus: Continual imitation learning for robot manipulation through unsupervised skill discovery. In *2024 IEEE International Conference on Robotics and Automation (ICRA)*, pages 537–544. IEEE, 2024. 2, 3, 6
 - [45] Yixiao Wang, Yifei Zhang, Mingxiao Huo, Ran Tian, Xiang Zhang, Yichen Xie, Chenfeng Xu, Pengliang Ji, Wei Zhan, Mingyu Ding, et al. Sparse diffusion policy: A sparse, reusable, and flexible policy for robot learning. *arXiv preprint arXiv:2407.01531*, 2024. 2
 - [46] Yating Wang, Haoyi Zhu, Mingyu Liu, Jiange Yang, Hao-Shu Fang, and Tong He. Vq-vla: Improving vision-language-action models via scaling vector-quantized action tokenizers. *arXiv preprint arXiv:2507.01016*, 2025. 2, 3
 - [47] Zihao Wang, Shaofei Cai, Zhancun Mu, Haowei Lin, Ceyao Zhang, Xuejie Liu, Qing Li, Anji Liu, Xiaojian Shawn Ma, and Yitao Liang. Omnijarvis: Unified vision-language-action tokenization enables open-world instruction following agents. *Advances in Neural Information Processing Systems*, 37:73278–73308, 2024. 2
 - [48] Hongtao Wu, Ya Jing, Chilam Cheang, Guangzeng Chen, Jiafeng Xu, Xinghang Li, Minghuan Liu, Hang Li, and Tao Kong. Unleashing large-scale video generative pre-training for visual robot manipulation. *arXiv preprint arXiv:2312.13139*, 2023. 2
 - [49] Zhiyu Wu, Xiaokang Chen, Zizheng Pan, Xingchao Liu, Wen Liu, Damai Dai, Huazuo Gao, Yiyang Ma, Chengyue Wu, Bingxuan Wang, et al. Deepseek-vl2: Mixture-of-experts vision-language models for advanced multimodal understanding. *arXiv preprint arXiv:2412.10302*, 2024. 2
 - [50] Jonathan Yang, Chuyuan Kelly Fu, Dhruv Shah, Dorsa Sadigh, Fei Xia, and Tingnan Zhang. Bridging perception and action: Spatially-grounded mid-level representations for robot generalization. *arXiv preprint arXiv:2506.06196*, 2025. 2
 - [51] Zhenjie Yang, Yilin Chai, Xiaosong Jia, Qifeng Li, Yuqian Shao, Xuekai Zhu, Haisheng Su, and Junchi Yan. Drivemoe: Mixture-of-experts for vision-language-action model in end-to-end autonomous driving. *arXiv preprint arXiv:2505.16278*, 2025. 2
 - [52] Jiawen Yu, Hairuo Liu, Qiaojun Yu, Jieji Ren, Ce Hao, Haitong Ding, Guangyu Huang, Guofan Huang, Yan Song, Panpan Cai, et al. Forcevla: Enhancing vla models with a force-aware moe for contact-rich manipulation. *arXiv preprint arXiv:2505.22159*, 2025.
 - [53] Rongyu Zhang, Menghang Dong, Yuan Zhang, Liang Heng, Xiaowei Chi, Gaole Dai, Li Du, Yuan Du, and Shanghang Zhang. Mole-vla: Dynamic layer-skipping vision language action model via mixture-of-layers for efficient robot manipulation. *arXiv preprint arXiv:2503.20384*, 2025. 2

- [54] Wenyao Zhang, Hongsi Liu, Zekun Qi, Yunnan Wang, Xinqiang Yu, Jiazhao Zhang, Runpei Dong, Jiawei He, Fan Lu, He Wang, et al. Dreamvla: a vision-language-action model dreamed with comprehensive world knowledge. *arXiv preprint arXiv:2507.04447*, 2025. [2](#)
- [55] Han Zhao, Wenxuan Song, Donglin Wang, Xinyang Tong, Pengxiang Ding, Xuelian Cheng, and Zongyuan Ge. More: Unlocking scalability in reinforcement learning for quadruped vision-language-action models. *arXiv preprint arXiv:2503.08007*, 2025. [2](#)
- [56] Ruijie Zheng, Ching-An Cheng, Hal Daumé III, Furong Huang, and Andrey Kolobov. Prise: Learning temporal action abstractions as a sequence compression problem. *CoRR*, 2024. [2](#)

Continually Evolving Skill Knowledge in Vision Language Action Model

Supplementary Material

Appendix

A. Overview

In the Appendix, we will provide the following details of the method and more results in experiments:

- Sampling and learning process of Dirichlet Process-based models for knowledge evolving in Sec. B
- Implementation details of our model structure, training process and loss definition in Sec. C
- Additional experiments and visualizations in Sec. D.
- Additional discussions in Sec. E.

B. Dirichlet Process-based Models Details

Dirichlet Process Sampling. To sample random probability measure G from Dirichlet Process, let G_0 be a base distribution, and $\alpha > 0$ be a concentration parameter. Then DP sampling could be represented as:

$$G \sim DP(\alpha, G_0) \quad (11)$$

A method known as the Stick-Breaking Process (SBP) [37] is employed to generate DP samples. More specifically, the construction introduces an infinite sequence of latent variables that recursively allocate portions of a “stick.” First, draw an infinite sequence of independent weights

$$v_k \sim \text{Beta}(1, \alpha), \quad k = 1, 2, \dots, \quad (12)$$

Where $\text{Beta}(1, \alpha)$ denotes the Beta distribution with shape parameters. The mixing proportions are defined by:

$$\pi_1 = v_1, \quad \pi_k = v_k \prod_{j=1}^{k-1} (1 - v_j), \quad k \geq 2. \quad (13)$$

Intuitively, v_1 determines the fraction of the stick broken off for the first atom; then v_2 determines the fraction of the remaining stick assigned to the second atom, and so on. In parallel, draw an independent sequence of atoms:

$$\theta_k^* \sim G_0, \quad (14)$$

which represent the locations at which the DP places point masses. Having $\delta_{\theta_k^*}(\theta) \begin{cases} 1, & \text{if } \theta = \theta_k^*, \\ 0, & \text{otherwise.} \end{cases}$, we could finally represent $G \sim DP(\alpha, G_0)$ as:

$$G = \sum_{k=1}^{\infty} \pi_k \delta_{\theta_k^*} \quad (15)$$

This formulation guarantees two fundamental properties of the Dirichlet Process: 1) G can contain a potentially infinite number of mixture components, since the stick-breaking process generates an unbounded sequence of weights. 2) the resulting random measure is discrete, since its mass is fully allocated across a countable sequence of atoms.

In our knowledge space modeling, we adopt a Normal–Wishart base distribution as G_0 , ensuring that each task or skill component in the knowledge space is represented by a multivariate Gaussian distribution.

Variational inference of the Knowledge Space. Our goal is to approximate posterior $p(\mathbf{v}, \Theta, \beta \mid \mathbf{Z})$ over cluster assignments v_n , component parameters θ_k , and stick-breaking weights β , where $\mathbf{Z} = \{z_1, \dots, z_N\}$ denotes the observed data, and $\Theta = \{\theta_1, \dots, \theta_K\}$ represents all component-specific parameters. Direct computation of this posterior is infeasible, so we introduce a factorized variational distribution:

$$q(\mathbf{v}, \Theta, \beta) = \prod_{n=1}^N q(v_n) \prod_{k=1}^K q(\theta_k) \prod_{k=1}^K q(\beta_k), \quad (16)$$

The posterior $p(\mathbf{v}, \Theta, \beta \mid \mathbf{Z})$ could then be approximated by minimizing the Kullback–Leibler (KL) divergence $\text{KL}(q(\mathbf{v}, \Theta, \beta) \parallel p(\mathbf{v}, \Theta, \beta \mid \mathbf{Z}))$. According to [5], the KL divergence can be rewritten as

$$\begin{aligned} \text{KL}(q \parallel p) = & - \underbrace{\mathbb{E}_q[\log p(\mathbf{Z}, \mathbf{v}, \Theta, \beta)] - \mathbb{E}_q[\log q(\mathbf{v}, \Theta, \beta)]}_{\text{ELBO}} \\ & + \log p(\mathbf{Z}). \end{aligned} \quad (17)$$

Since $\log p(\mathbf{Z})$ is constant, minimizing KL is equivalent to maximizing the Evidence Lower Bound (ELBO). The ELBO can be expanded as introduced in [5, 13]:

$$\begin{aligned} \text{ELBO}(q) = & \underbrace{\mathbb{E}_q[\log p(\mathbf{Z} \mid \mathbf{v}, \Theta)]}_{\text{expected data likelihood}} + \underbrace{\mathbb{E}_q[\log p(\mathbf{v} \mid \beta)]}_{\text{assignment prior}} \\ & + \underbrace{\mathbb{E}_q[\log p(\Theta \mid G_0)]}_{\text{component prior}} + \underbrace{\mathbb{E}_q[\log p(\beta)]}_{\text{stick-breaking prior}} \\ & - \underbrace{\mathbb{E}_q[\log q(\mathbf{v})]}_{\text{assignment entropy}} - \underbrace{\mathbb{E}_q[\log q(\Theta)]}_{\text{component entropy}} \\ & - \underbrace{\mathbb{E}_q[\log q(\beta)]}_{\text{weight entropy}}. \end{aligned} \quad (18)$$

We can iteratively update each factor while holding the others fixed, thereby monotonically increasing the ELBO. **Memoized Variational Bayes.** Building on the above

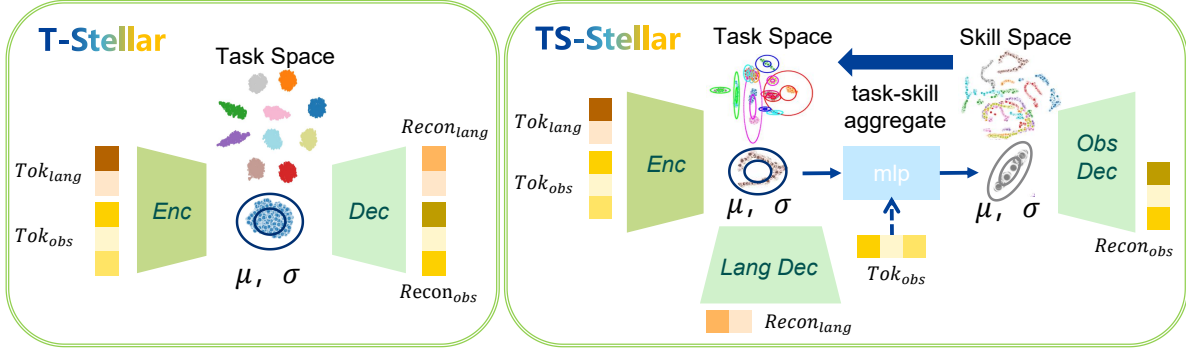


Figure 6. **VAE structure of T-Stellar and TS-Stellar.** T-Stellar adopts a standard VAE framework for task-level modeling, whereas TS-Stellar introduces a hierarchical structure for joint task-skill modeling.

principle, Memoized Variational Bayes (memoVB) [13] efficiently performs variational inference for DPMM or HDP models. Specifically, memoVB follows the below steps to update parameters given the observation data z :

- **Local updates:** For each data point z_n , the variational assignment distribution $q(v_n)$ is updated based on the current estimates of the component parameters θ and the stick-breaking weights β . These updates maximize the ELBO with respect to $q(v_n)$, corresponding to the expected data likelihood, the assignment prior, and the assignment entropy in Eq. (18).
- **Global updates:** The component parameters $q(\theta_k)$ and the stick-breaking weights $q(\beta_k)$ are updated using the aggregated information from all data points z weighted by their current assignment probabilities. These updates maximize the ELBO with respect to the global factors, corresponding to the expected data likelihood, the component prior, the stick-breaking prior, and the entropies of $q(\theta_k)$ and $q(\beta_k)$ in Eq. (18).
- **Component management:** This step manages the birth of new components and the pruning or merging of low-contribution ones. New components are added when doing so increases the ELBO, while components with minimal contribution can be pruned or merged. To reduce the computational cost of revisiting many data points, memoVB caches statistics of inactive components, updating only the active ones and thus improving efficiency while preserving the model’s flexibility.

Through this alternating local-global optimization and dynamic component management, memoVB efficiently maximizes the ELBO while preserving the nonparametric flexibility of the model.

C. Implementation Details

Network Architecture. As discussed in the main paper, Stellar VLA consists of a pretrained vision-language encoder, a VAE encoder-decoder, and a diffusion-based trans-

Algorithm 1 Joint Evolution of Task-centric Latents and Knowledge Space

- 1: Initialize knowledge-space distribution Θ using the DP-based model
- 2: Initialize VAE parameters ϕ, ψ
- 3: Initialize knowledge-space buffer \mathcal{B}
- 4: **for** training data x at iteration $t = 1, \dots, T$ **do**
- 5: Sample latent $z \sim q_\phi(z | x)$
- 6: Compute losses $L_{\text{recon}}, L_{\text{kl}}$
- 7: Update VAE $\phi, \psi \leftarrow \phi, \psi - \eta \nabla_{\phi, \psi} (L_{\text{recon}} + L_{\text{kl}})$
- 8: Update buffer $\mathcal{B} \leftarrow \mathcal{B} \cup \{x\}$
- 9: **if** $t \bmod N_{\text{dp}} = 0$ and $t < N_{\text{max}}$ **then**
- 10: Sample K_{know} latent points $\{z_i\}_{i=1}^{K_{\text{know}}} \sim q_\phi(z | x), x \sim \mathcal{B}$
- 11: Update knowledge parameters Θ as in Sec. B
- 12: **end if**
- 13: **end for**

former action head with mixture-of-experts (MoE). The network takes language instruction, observation images, and proprioceptive states as input. The language instruction is encoded using CLIP [33] and projected into a 1024-dimensional embedding tok_{lang} . Observation images are processed by a FiLM [32]-conditioned ResNet that injects language features, followed by a linear projection producing N image tokens tok_{obs} . Proprioceptive inputs are also linearly projected to 1024-dimensional token tok_{proprio} .

The VAE encoder is a MLP that takes the concatenation of $tok_{\text{lang}}, tok_{\text{obs}}$, and tok_{proprio} and infers the Gaussian parameters (μ, σ) of the task-centric latent space. z is then sampled via reparameterization. For TS-Stellar, which models both task- and skill-level structure, the latent vector and visual embeddings are further processed by an additional linear layer to obtain skill-level Gaussian parameters $(\mu_{\text{skill}}, \sigma_{\text{skill}})$. The architectural differences of VAE module between T-Stellar and TS-Stellar are shown in Fig. 6.

Table 5. **Performance of trained from scratch models on the LIBERO benchmark.** Results are reported in percentages. The best performance is shown in **bold**.

tasks	metrics	UniVLA [6] (scratch)	MoDE [35] (scratch)	T-Stellar (scratch, ours)	TS-Stellar (scratch, ours)
LIBERO-goal	FWT (\uparrow)	2.4	68.5	81.9	78.5
	NBT (\downarrow)	2.4	33.6	19.3	21.9
	AUC (\uparrow)	0.3	38.5	63.2	58.3
	Final SR (\uparrow)	0.0	36.0	66.8	64.3
LIBERO-long	FWT (\uparrow)	6.2	66.6	78.6	74.7
	NBT (\downarrow)	6.1	45.4	44.3	37.9
	AUC (\uparrow)	0.9	28.4	41.2	41.7
	Final SR (\uparrow)	0.0	18.6	31.9	36.8

Table 6. **Success rate on the LIBERO benchmark in the multitask setting.** Results are reported as percentages, with the best scores shown in **bold**. All evaluated models perform well, with Stellar VLA variants achieving the best overall performance.

tasks	UniVLA [6] (fine-tuned)	MoDE [35] (fine-tuned)	MoDE [35] (scratch)	T-Stellar (scratch, ours)	TS-Stellar (scratch, ours)
LIBERO-goal	95.6	90.7	96.6	96.5	96.7
LIBERO-long	92.0	94.0	92.0	94.4	94.3

The task-centric latent z is 10-dimensional. After combining z with the knowledge-space prior (described in Sec. 3.4), a linear layer maps the result to the 1024-dimensional knowledge token tok_{know} . In the diffusion-based transformer action head, tok_{know} , tok_{lang} , tok_{obs} , $tok_{proprio}$, tok_{noise} , and the action noise tokens tok_{act} are jointly fed into the denoising transformer. Final action sequence is acquired from the output tok_{act} through linear layers. Same as MoDE [35], Stellar VLA uses EDM [17]-based diffusion framework for the denoising process.

For the transformer MoE, as described in Sec. 3.4, the tokens tok_{know} , tok_{lang} , and tok_{noise} are concatenated and used as inputs to the router, which determines expert selection for all tokens.

Joint Evolution Process of Task-centric latents and Knowledge Space. During training, the task-centric representation z and the knowledge space evolve jointly. To illustrate this co-evolution, we summarize the training process in Algorithm 1.

At the beginning of training, the DP-based model (DPMM or HDP) initializes the knowledge-space distribution Θ . As training proceeds, the VAE is updated continuously through the reconstruction loss L_{recon} and KL divergence L_{kl} described in Sec. 3.3. Meanwhile, knowledge space maintains its own buffer that stores data during training. Every N_{dp} iterations, the knowledge space samples K_{know} items from the buffer and encodes them using the VAE encoder to obtain a set of latent observations $\{z\}$. The DP-based model then updates its distribution parameters Θ using variational inference described in Sec. B.

Because Θ is updated periodically, the KL term L_{kl} in subsequent VAE updates pulls the latent representation z toward the updated knowledge-space distribution. Through this iterative process, Stellar VLA achieves a mutually reinforcing co-evolution between the task-centric representation and the knowledge space.

Note that the buffer used for updating knowledge space differs from the memory buffer for ER-based CIL described in Sec. 3.1. It is used solely for updating DP-based model during training and is cleared after each task, ensuring no additional long-term storage overhead.

Training Losses. The overall training objective consists of the VAE representation losses and the action-head prediction losses. The VAE is optimized using the reconstruction loss L_{recon} and KL divergence L_{kl} as described in Sec. 3.3.

For the action head, the denoising module is trained via a score-matching loss [43]:

$$\mathcal{L}_{SM} = \mathbb{E}_{\mathbf{a}, \epsilon, \sigma} \left[\alpha(\sigma) \left\| D_{\omega}(\mathbf{a} + \sigma\epsilon, \{Tok_s\}, \sigma) - \mathbf{a} \right\|_2^2 \right], \quad (19)$$

where D_{ω} is the denoising transformer, $\{Tok_s\}$ denotes all input observation tokens, σ is the noise level, and $\alpha(\sigma)$ is a noise-dependent weighting term.

To prevent expert collapse in the MoE transformer, a load-balancing loss [9] is applied:

$$L_{bal} = \sum_{i=1}^{N_e} p_i f_i, \quad (20)$$

where N_e is the number of experts, p_i is the router’s av-

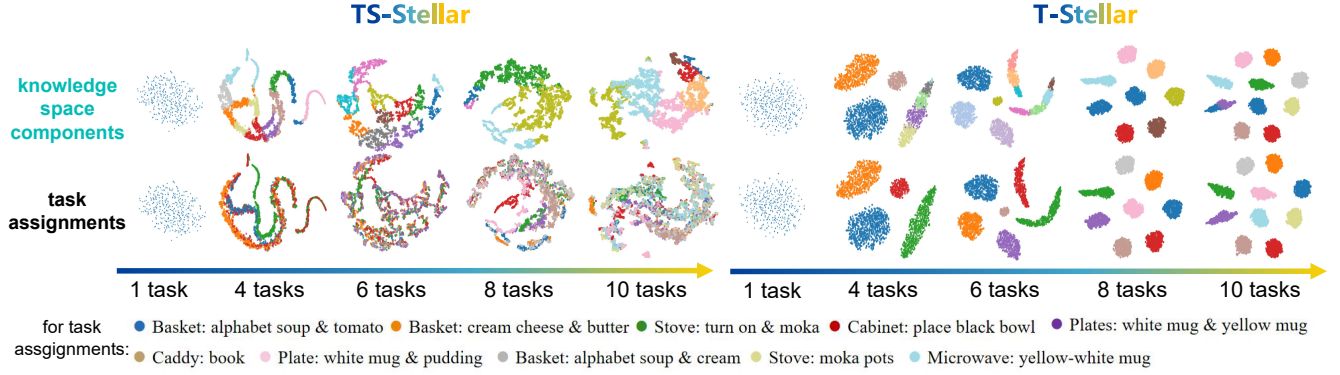


Figure 7. **Visualization of knowledge space components in Stellar VLA.** Task labels are shown in the bottom row, while dynamic knowledge-space components are only color-coded. Comparing knowledge space clusters with task labels, TS-Stellar groups related tasks into shared skill components, and T-Stellar learns components that largely align with true task assignments.

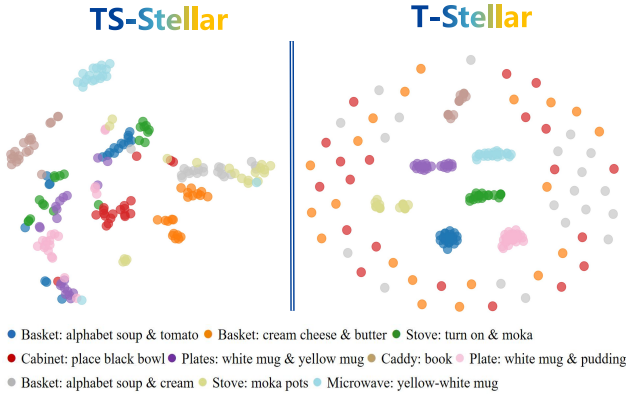


Figure 8. **T-SNE visualization of knowledge-routed expert activation patterns on LIBERO-long.** Both TS-Stellar and T-Stellar exhibit a certain degree of task-specific expert routing patterns.

erage assignment probability, and f_i is the empirical usage frequency of expert i . The final training objective is

$$L_{\text{total}} = L_{\text{recon}} + L_{\text{kl}} + L_{\text{SM}} + L_{\text{bal}}. \quad (21)$$

Training Details. In continual imitation learning, Stellar VLA is trained on each task with AdamW optimizer for 10K steps, totally taking about 30 hours on a single NVIDIA H200 GPU for 10 tasks. We use a batch size of 128 with a learning rate of $1e-4$ and weight decay of 0.05.

For comparison baselines, pretrained and trained from scratch MoDE [35] are also trained for 10K steps on each task, and keeps the same setting as ours. As for UniVLA [6], since 10-task LIBERO benchmark is reported to be trained for 30K steps under the multitask setting, we train UniVLA with 128 batch size for 3K steps on each task, taking about 40 hours on 2 NVIDIA H200 GPUs for 10 tasks.

D. Additional Experiments

All Scratch Model Results on LIBERO. For fair comparison with MoDE, Stellar VLA uses a single image token via global pooling. To align all baselines with our setting, we report all from-scratch results here for UniVLA [6], MoDE [35], TS-Stellar, and T-Stellar in Tab. 5. For UniVLA, only the VLA backbone is trained from scratch, and its latent-action tokenizer remains pretrained. As shown, our method achieves the strongest performance across all from-scratch models. Since UniVLA (scratch) shows near-zero success and fails to learn meaningful manipulation behavior, we do not include its LIBERO-30* results, and UniVLA (scratch) does not appear in the main text.

Multitask Learning Results on LIBERO. We also report multitask results on LIBERO-goal and LIBERO-long to demonstrate that the evaluated VLA models [6, 35] are strong baselines, as shown in Tab. 6. Since MoDE [35] only provides results on LIBERO-long, we reproduce it on LIBERO-goal for completeness. The results show that Stellar VLA also achieves strong performance in the multitask setting. Together with the main experiments, these findings indicate that although UniVLA and MoDE perform well under multitask training, they still show notable degradation in the continual-learning setting, underscoring the challenges that CIL poses for VLA models.

More Visualization for Knowledge Evolution. To illustrate the role of knowledge space, Fig. 7 further compares the Gaussian components learned by the DP-based model with the ground-truth task labels. For TS-Stellar, the learned components primarily follow the distribution of the latent representations, effectively forming a self-supervised skill-level partition as discussed in Sec. 4.4. For T-Stellar, although some intra-task substructures may emerge during continual training, the final components largely align with the true task labels, demonstrating accurate modeling of

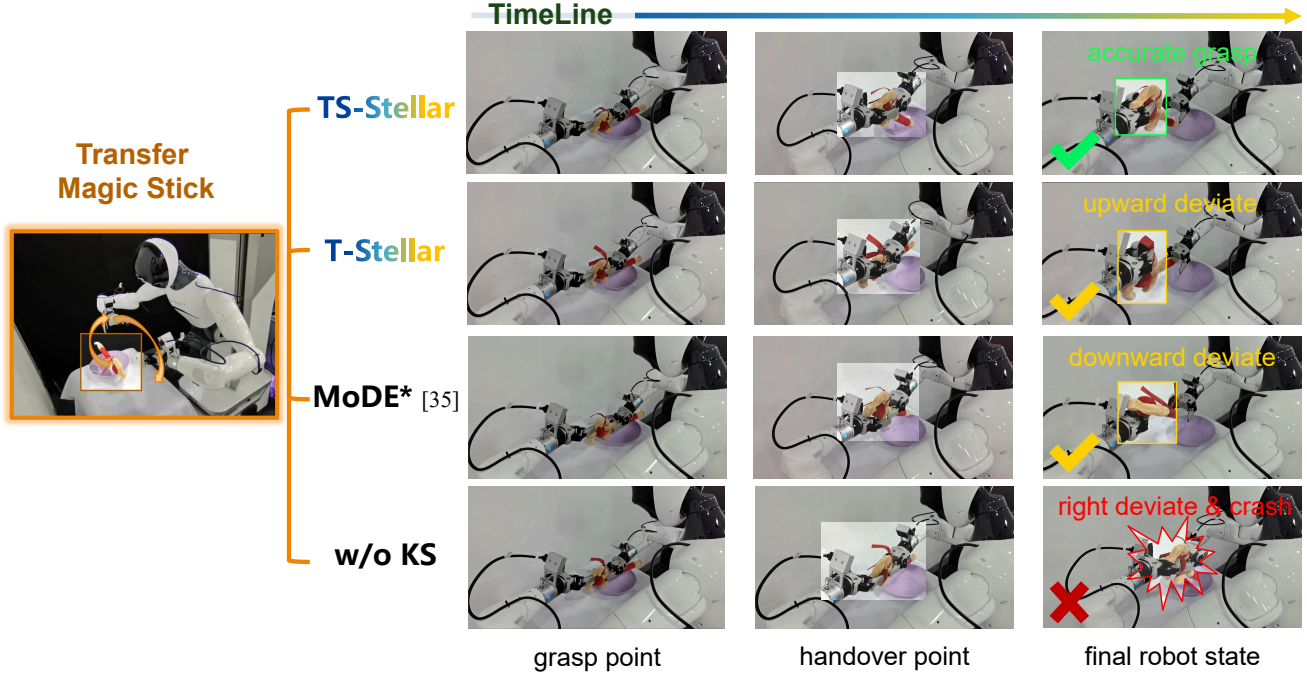


Figure 9. **Behavior visualization on “Transfer Magic Stick” after training on “Handover Toy”.** During the transfer, TS-Stellar shows the most accurate dual-arm alignment. T-Stellar and MoDE* exhibit mild misalignments but still complete the grasp, whereas w/o KS suffers a severe rightward deviation that causes a collision and finally fails.

task-level structure.

Expert Usage Analysis. To examine whether the proposed knowledge-guided expert routing enables task specialization, we follow the visualization procedure of [2] to analyze expert activation patterns. After continual training on LIBERO-long, we record the expert-selection frequencies of Stellar VLA when evaluated on all previously learned tasks. Expert activations from each episode are concatenated into a feature vector, and 20 episodes are sampled per task. Results are visualized using t-SNE, as shown in Fig. 8.

Both TS-Stellar and T-Stellar exhibit some degree of task-dependent expert pattern clustering. TS-Stellar shows partial overlap across tasks, suggesting shared behavioral patterns in certain trajectories. In T-Stellar, most tasks form distinct clusters, while a few appear mixed in 2D space, likely due to projection artifacts given the high dimensionality of the activation vectors. Overall, these results demonstrate that knowledge-guided expert routing could induce task specialization.

More Task Behavior Comparison. In real-world experiments, three tasks are designed: 1) “Transfer Magic Stick”: Pick up the magic stick with the right arm, and transfer it to the left arm. 2) “Pick up Bag”: Pick up the bag with both arms. 3) “Handover Toy”: Pick up the toy with the right arm, and handover to the left arm. In addition to the behavior analysis of “Pick up Bag” task in the main text, We visu-

alize the execution of “Transfer Magic Stick” in Fig. 9. Although “Handover Toy” and “Transfer Magic Stick” share similar handover patterns, the latter requires more precise alignment. As shown, TS-Stellar reliably achieves accurate dual-arm transfer, while T-Stellar and MoDE* exhibit noticeable grasp-position deviations. Although these models still complete the task, such offsets may cause failures in edge cases due to unstable grasping. W/o KS suffers more severe misalignment that leads to collisions and task failure. Evaluating on “Transfer Magic Stick” after training on “Handover Toy” further confirms the robustness of TS-Stellar in handling complex manipulation.

E. Limitation and Future Works

As detailed in Sec. C, Stellar VLA adopts a small pre-trained VLM for vision–language encoding, with an overall model size of around 1B parameters. This limited capacity may hinder the model’s ability to interpret subgoal-level information embedded in language or visual observations, thereby restricting its few-shot adaptability on new tasks and limiting rapid forward transfer. TS-Stellar, in particular, requires further evaluation in such generalization scenarios. In future work, we plan to investigate our approach using larger-scale pretrained VLMs and action prediction networks, and to explore extensions toward continual policy generalization across diverse tasks.